Three-Dimensional Analysis of Submacular Perforating Scleral Vessels by Enhanced Depth Imaging Optical Coherence Tomography

Rothenbuehler, Simon P ; Maloca, Peter ; Scholl, Hendrik P N ; Gyger, Cyrill ; Schoetzau, Andreas ; Kuske, Lorenz ; Mosimann, Nathanael ; Zweifel, Sandrine A ; Barthelmes, Daniel ; Tufail, Adnan ; Hasler, Pascal W

DOI: https://doi.org/10.1097/IAE.0000000000001686

THREE-DIMENSIONAL ANALYSIS OF SUBMACULAR PERFORATING SCLERAL VESSELS BY ENHANCED DEPTH IMAGING OPTICAL COHERENCE TOMOGRAPHY

SIMON P. ROTHENBUEHLER, MD,* PETER MALOCA, MD,*† HENDRIK P. N. SCHOLL, MD, MA,*‡ CYRILL GYGER, MSc,* ANDREAS SCHOETZAU, MSc,§ LORENZ KUSKE, MD,* NATHANAEL MOSIMANN, MD,* SANDRINE A. ZWEIFEL, MD,¶ DANIEL BARTHELMES, MD, PHD,¶ ADNAN TUFAIL, MD, FRCOphth,† PASCAL W. HASLER, MD*

Purpose: To analyze submacular perforating scleral vessels (PSVs) using enhanced depth imaging spectral domain optical coherence tomography (EDI-SDOCT).

Methods: Twenty-two eyes of 11 healthy women were included in this retrospective study. Central EDI-SDOCT scans ($3 \times 4.5 \times 1.9$ mm, 13.5 mm^2 scan area) were acquired and postprocessed by denoising, manual sclera segmentation, and PSV investigated by five graders.

Results: Mean age was 22.4 ± 6.2 years. Mean refractive error was −0.44 ± 0.8 diopters. Mean axial length was 23.08 ± 0.63 mm. The coefficient of agreement for grading was good. Mean number of submacular PSVs was 0.33 ± 0.2 per mm^2 (range from 0 to 9 per eye). Subfield analysis showed 0.2 ± 0.5 (range 0–2) and 2.1 ± 1.8 (range 0–7) vessels, respectively, for central 1-mm diameter and 3-mm diameter. Quadrant analysis showed 0.7 ± 0.9, 0.5 ± 0.9, 0.3 ± 0.6, and 0.4 ± 0.6 vessels, respectively for superior, inferior, nasal, and temporal quadrants. Total number of PSV showed no significant side difference (median difference 0.5, confidence interval −3.0 to 3.0, $P = 0.94$) or an influence of axial length ($P = 0.16$).

Conclusion: This is the first description of three-dimensional EDI-SDOCT visualization of submacular PSV in healthy eyes. This method allows for in vivo imaging of a critical component of outer retinal perfusion at the posterior pole.

RETINA 0:1–7, 2017

Advances of optical coherence tomography (OCT) such as enhanced depth imaging in spectral domain OCT (EDI-SDOCT) and swept-source OCT (SSOCT) have improved visualization depth and offer to look beyond the retina at deeper ocular structures.[1]

Swept-source OCT has less sensitivity roll-off with depth and allows for a deeper range of imaging.[2] Enhanced depth imaging uses a closer scanning position to the eye to create an inverted SDOCT image with the advantage of better depth sensitivity.[3] When the choroid and retinal pigment epithelium are thin or absent, visualization of the sclera and retrobulbar tissue is possible with enhanced depth imaging as reported by Invernizzi et al[4] in cases of pathologic myopia. In healthy eyes, because of attenuation of the OCT signal with increasing depth, these structures have been difficult to visualize.

Choroidal blood flow is the highest of any tissue per weight unit in the human body and exceeds the retinal circulation by a factor of 20.[5] Over 70% of overall blood flow in the eye is directed to the choroid.[6] Our understanding of the choroidal blood supply is limited in part because of our limited ability to adequately visualize it. Better imaging and better understanding of this critical zone can focus on the individual potential for the exchange of fluids, oxygen, and nutrients, which might be of importance in the pathogenesis of diseases such as age-related macular degeneration, central serous chorioretinopathy, staphyloma formation in pathologic myopia,[1] and diabetic retinopathy.[7]

Originating from the ophthalmic artery, multiple branches of posterior ciliary arteries (PCAs) reach the back of the eyeball. A subgroup of the PCAs, the 15 to 20 short posterior ciliary arteries (SPCAs) transverse

the sclera around the optic nerve to provide crucial circulation to the optic nerve head and the posterior choroid.[8] Hayreh,[9] after his extensive studies on the subject, argues that the choroidal circulation is a strictly segmental end-arterial system and introduced the concept of watershed zones located between the various SPCAs. Multiple sectorial watershed zones meet in the submacular region, presumably making the macula and the avascular zone of the fovea vulnerable to ischemia under certain conditions.[9]

Perforating scleral vessels (PSVs) have been visualized as linear hyporeflective structures at the level of the sclera by EDI-SDOCT and swept-source OCT in pathologic myopia as reported by Pedinielli et al[10] and Ohno-Matsui et al.[11] More recently, perforating scleral vessels have been investigated in connection with lacquer cracks in pathologic myopia by Querques et al.[12] They have been hypothesized to act as "locus minoris resistentiae," leading to scleral expansion and lacquer crack formation. Because of low signal-to-noise ratio, the visualization of PSVs in emmetropic eyes has been more problematic to date.[9]

The PCAs, and therefore PSVs, are a critical component of blood supply of the outer retina of the posterior pole and the optic nerve head. Moreover, their location and number in the submacular region could be a contributing factor in the development and course of certain retinal disorders.

The purpose of this retrospective study was to explore the distribution of submacular PSVs in a set of healthy eyes by means of conventional EDI-SDOCT. Image postprocessing algorithms and three-dimensional rendering used in this study[13,14] allow for in vivo visualization and quantification of vessels, and potentially expand our knowledge on choroidal perfusion at the posterior pole.

From the *OCTlab, Department of Ophthalmology, University Hospital Basel, University of Basel, Basel, Switzerland; Medical Retina Department, †Moorfields Eye Hospital, NHS Foundation Trust, London, United Kingdom; ‡Wilmer Eye Institute, Johns Hopkins University, Baltimore, Maryland; §Department of Biomedical Statistics, University of Basel, Basel, Switzerland; and ¶Department of Ophthalmology, University Hospital Zurich, University of Zurich, Zurich, Switzerland.

Supported in part by prize money of the Swiss VitreoRetinal Group, Retina Award 2015.

A. Tufail has been on advisory boards for Novartis, Pfizer, GSK, Thrombogenics, Bayer, and Allergan. The remaining authors have no conflicting interests to disclose.

P. Maloca and S. P. Rothenbuehler contributed equally to this work.

Supplemental digital content is available for this article. Direct URL citations appear in the printed text and are provided in the HTML and PDF versions of this article on the journal's Web site (www.retinajournal.com).

P. Maloca is owner of intellectual property on speckle noise analysis technology discussed in this work.

Reprint requests: Simon P. Rothenbuehler, MD, OCT Research Laboratory OCTlab, Department of Ophthalmology, University Hospital Basel, Mittlere Strasse 91, CH-4056 Basel, Switzerland; e-mail: simon.rothenbuehler@usb.ch

Methods

Population

In this retrospective study, we included 22 eyes of 11 healthy women. Inclusion criteria were age above 18 years, emmetropia or less than 3 diopters of refractive error, good central fixation, and best-corrected visual acuity of 20/20 or better. Exclusion criteria were presence of ocular disease, history of ocular trauma, intraocular or extraocular surgery, elevated intraocular pressure, family history of eye disease, medical history of smoking, and systemic or ocular medication or coexisting systemic disease such as diabetes mellitus, hypertension, or cardiovascular disease. Informed consent was obtained from the subjects after explanation of the nature and possible consequences of the study. Before measurements, best-corrected visual acuity and a comprehensive ophthalmic examination of all subjects was performed to exclude existing retinal or choroidal abnormalities. The study was approved by the ethical committee at the University of Basel, Switzerland, and is in accordance with the tenets of the Declaration of Helsinki and in compliance with Swiss patient data protection regulations.

Enhanced Depth Imaging Optical Coherence Tomography Examination

The OCT examination was carried out by an experienced operator using a Heidelberg Spectralis SDOCT device (Spectralis HRA 2, Version 6.0.10.0; Heidelberg Engineering, Heidelberg, Germany). Volume scans of 4.5 mm × 3 mm × 1.9 mm were acquired in a horizontal raster line pattern of 261 B-scans with 12 μm spacing. The enhanced depth imaging mode was enabled together with automatic averaging of 20 B-scans.

Image Postprocessing and Speckle Noise Removal

The open source program ImageJ (available at the public domain at http://imagej.nih.gov, last accessed on November 12, 2016) was used for image postprocessing. The single B-scans of the acquired volume data were normalized using the shadow removal and contrast enhancement method.[15] The aspect ratio was normalized to get an equal representation in all three dimensions. The imaging data was then processed by an algorithm for speckle noise removal with preservation of structure information as described elsewhere.[14]

An overdriving histogram equalization was used for better separation of hyperreflective and hyporeflective areas in the volume data based on the contrast limited adaptive histogram equalization method. Postprocessing was finished by two subsequent denoising runs. Figure 1 depicts the postprocessing pipeline with section D and E showing examples before and after the denoising processing. A video showing the image postprocessing and three-dimensional visualization of the data is available as **Supplemental Digital Content 1** (see **Video**, http://links.lww.com/IAE/A648).

Identification of Perforating Scleral Vessels

Speckle-free OCT imaging data was then further analyzed using the program ImageJ. Within the volumes, a region of interest (ROI) was manually defined with the anterior border at the level of the hyperreflective band corresponding to the RPE and the posterior border in the sclera. This ROI was applied to all individual volume scans.

Traversing hyporeflective areas in the ROI were identified as choroidal vessel formations based on international OCT nomenclature. Hyporeflective spaces corresponding to choroidal vessels were then segmented by threshold filtering in all volume data sets as described previously.[13] Perforating scleral vessels are therefore visualized as protruding vessel stumps at the posterior border of the ROI, as depicted in Figures 1F and 2.

Three-Dimensional Rendering

From the segmented vessels, a three-dimensional mesh was produced and rendering performed with Cinema 4D software, Release 16 (Maxon Computer GmbH, Friedrichsdorf, Germany).

Grading

Images of the posterior border of the ROI were then overlaid with a grid consisting of concentric rings of 1-mm and 3-mm diameter and sectors separating a total of five subfields centered on the fovea as shown in Figure 3. Manual grading of these images was performed by five different graders (P.M., P.W.H., S.P.R., L.K., and N.M.). Perforating scleral vessels had to be counted and mapped to the respective subfields of the grid, in the 4.5- by 3-mm scan area. The resulting number of vessels per subfield was derived from the agreement by most graders. In one case, where no majority was reached, the lower number of vessels was arbitrarily selected, based on the conservative assumption that artifacts might lead to a tendency of overestimation.

Statistics

Data analysis and descriptive statistics were performed using Excel for Mac 2011 version 15.19.1 and the software R version 3.1.3 (Project for Statistical Computing, available at: http://www.r-project.org). Intergrader agreement was assessed by calculation of the Light Kappa for agreement in the case of multiple raters and interpreted according to Landis and Koch.[16] For comparison of subfields regarding the number of PSVs, ratios of the mean number of vessels were calculated using Poisson regression, as described elsewhere.[17] The comparison of the right and left eyes regarding total number of vessels was done using Wilcoxon rank-sum test. Symmetry between the fellow eyes was assessed by nonparametric spearman correlation. Dependence of vessel number on axial length was analyzed by a linear mixed-effects model. Mixed-effects models were suitable tools for analysis of repeated measure data (here, left and right eye of each subject).

Results

A total of 22 eyes of 11 young healthy white female subjects were included in this study. Mean (mean ± SD) age was 22.4 ± 6.2 years. Mean refractive error was −0.44 ± 0.8 diopters, and mean axial length was 23.08 ± 0.63 mm. Perforating scleral vessels were counted by the graders and numbers combined for the 1 mm central subfield, 3 mm central subfield, and total 3- by 4.5-mm scan area, as well as the inferior, superior, nasal, and temporal quadrants as depicted in Figure 3. The independent grading performed by five physicians was analyzed by intergrader agreement. The coefficient of agreement was calculated and interpreted according to Landis and Koch,[16] with agreements for the different subfields ranging from 0.61 to 0.93 (95% confidence intervals) indicating a "substantial" to "almost perfect agreement."

The number of PSVs per eye ranged from 0 to 9 in the scanned area, with a mean of (mean ± SD) 4.5 ± 2.8. The number of PSVs per eye divided by the scan area of 13.5 mm^2 resulted the mean number of vessels at the posterior pole per mm^2 of 0.33 ± 0.2 (range 0–0.67). This figure of quantification is possibly an important vascular characteristic of the human eye.

To analyze the distribution of the vessels about the fovea, the mapping to the subfields of the grid depicted in Figure 3 showed the following results:

The mean number of PSVs in the central 1-mm diameter subfield was 0.2 ± 0.5 (range 0–2), for the 3-mm diameter subfield 2.1 ± 1.8 (range 0–7). Quadrants of the ring-shaped area defined by a 1-mm and 2-mm circle (Figure 3) showed the following mean

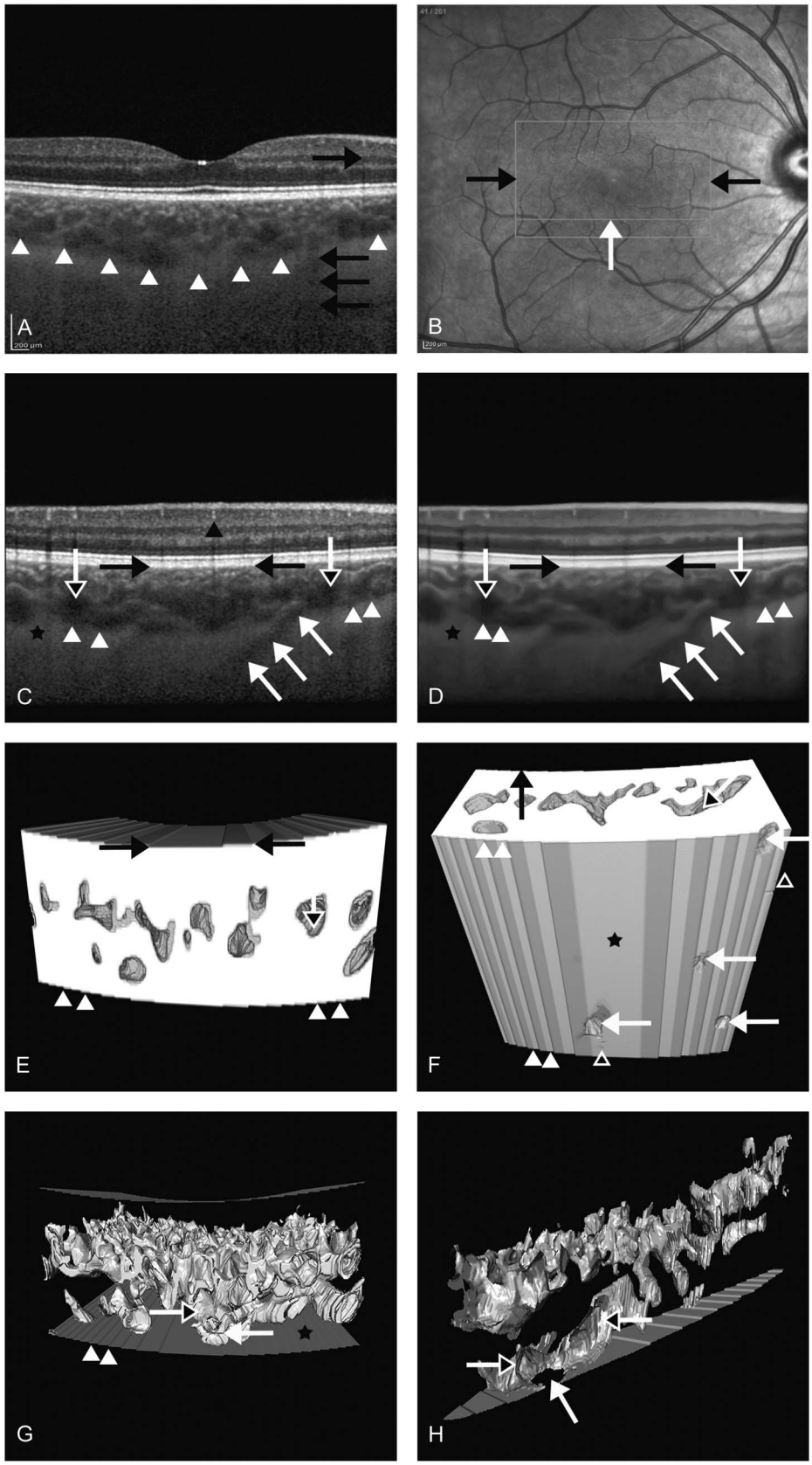

Fig. 1. Imaging of the choroidal compartment to illustrate PSVs by enhanced depth imaging spectral domain optical coherence tomography (EDI-SDOCT). **A.** B-scan of a healthy fovea showing a relatively sharp delineation of the choroid–sclera interface ([CSI], white arrowheads). In two locations, its continuity is broken by vertical shadows representing projection artifacts (black arrows) running in the direction of the scanning laser. In one instance, the artifact can be visibly traced to a retinal vessel (black arrow, pointing right). **B.** Scanning laser ophthalmoscopy image of the same eye with the green box (black arrows) indicating the scan area of the EDI-SDOCT and the position of the B-scan (white arrow) shown in (**C**). **C.** Corresponding original B-scan with the inner choroidal boundary delineated from the retina (black arrowhead) by a sharp line formed by the pigment epithelium-Bruch membrane complex (black arrows) and the outer choroidal boundary demarcated by the CSI (white arrowheads). A PSV is represented by a linear hyporeflective structure (white arrows) entering obliquely from below and interrupting the CSI. Scleral pillars protrude into the choroidal compartment as hyperreflective structures (black star) branching out to enclose hyporeflective spaces which correspond to large choroidal vessels (black headed arrow). **D.** Same image as in (**C**) after postprocessing with speckle noise removing algorithm. **E.** Inferior view of a three-dimensional visualization of the choroidal compartment after speckle noise removal with large choroidal vessels within (black headed arrow). The inner border (black arrows) is arbitrarily set at the pigment epithelium-Bruch membrane complex, and outer border is set slightly posterior to the CSI (white arrowheads). **F.** Posterior view of the same visualization as in (**F**) with the outer border (black star) interrupted by protruding PSVs (white arrows). Tiny surface irregularities do not correspond to PSVs but may represent artifacts (black arrowhead). **G.** Inner view of the same choroidal compartment illustrating larger vessel loops (black headed arrow) with focal attachment (white arrow) to the outer border (white arrow head), the remaining border clearly separated (black star). **H.** After virtual cutting of the same model, a connecting structure between the choroidal vessels (black headed arrows), and the outer border can be attributed to a PSV (white arrow).

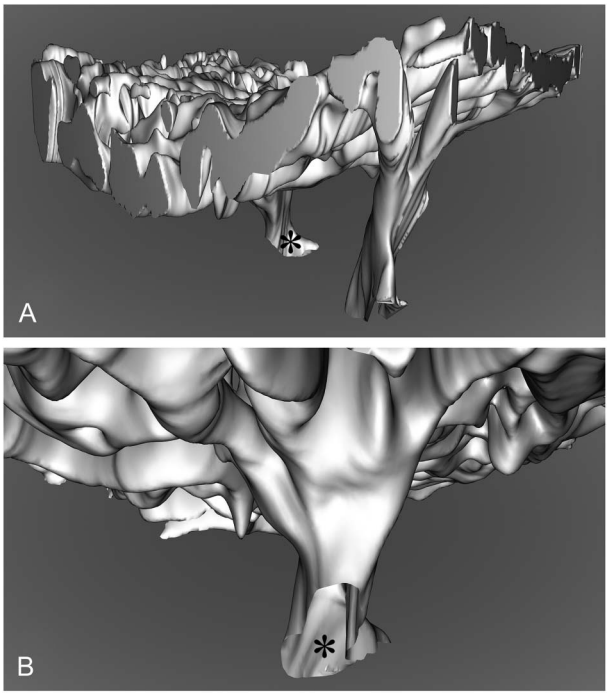

Fig. 2. Imaging of obliquely coursing PSVs by three-dimensional visualization with enhanced depth imaging spectral domain OCT. **A.** Three PSVs are shown protruding into the CSI (* marking the central vessel). **B.** Close-up showing the same entering vessel (*) in the center following a branching course into the choroid.

numbers of vessels: Superior 0.7 ± 0.9, inferior 0.5 ± 0.9, nasal 0.3 ± 0.6, and temporal 0.4 ± 0.6.

To check for a possible pattern of vessel distribution with a foveal, nasal, or temporal focus of density, the following comparison was performed: Comparison of the vessel number per surface area in 1-mm subfield and the surrounding donut ring up to 3 mm equaled a ratio of 0.98 with no significant difference (P = 0.99). A comparison of the opposite quadrants, nasal versus temporal and inferior versus superior, resulted in the ratios of 0.875 and 0.732, respectively, with no significant differences either (P = 0.994 and 0.863, respectively).

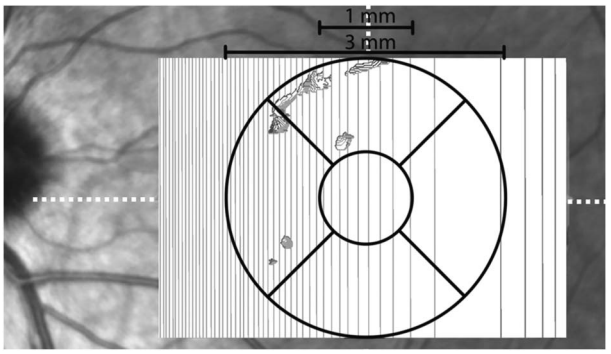

Fig. 3. Grid overlay centered on the fovea used for grading and data analysis with concentric rings at 1-mm and 3-mm diameter and quadrants.

Furthermore, comparison regarding the total number of vessels of the right and left eyes showed no significant difference (estimated median difference of 0.5, confidence interval −3.0 to 3.0, P = 0.94). Assessment of symmetry regarding total number of vessels in the fellow eyes showed no significant correlation (P = 0.94). There was no significant influence of axial length on the total number of vessels (P = 0.16).

Discussion

To our knowledge, this is the first study assessing posterior pole PSVs in healthy subjects using standard SDOCT. High-density volume scans with enhanced depth imaging OCT and suitable postprocessing make imaging and quantification of the PSVs possible. Three-dimensional visualization can reveal the characteristics of individual vessels entering the choroid as depicted in Figure 2.

Although indocyanine green angiography is the gold standard for visualization of the choroid to date, it is a two-dimensional imaging procedure with a limited extent of depth information for the deep choroidal vascular structures. Choroidal vessels are well identified in the early phase of indocyanine green angiography, but the vertical superposition of vessels complicate the accurate identification of the individual choroidal zone, and visualization may be blocked by melanin pigment and overlaying retinal or choroidal pathologies.[1] Furthermore, indocyanine green angiography angiography is an invasive procedure with rare but potential severe complications and therefore not ideal for repeated examinations. By contrast, in vivo three-dimensional OCT visualization of choroidal vessels may be performed as often as desired and offers a new perspective at a critical component of submacular ocular blood flow.

Perforating scleral vessels have been implicated in the pathogenesis of structural changes of the sclera as investigated by OCT and reported by Pedinielli et al[10] and Ohno-Matsui et al.[11] More recently, Querques et al[12] reported on the formation of lacquer cracks in pathologic myopia. Assessed by indocyanine green angiography angiography, Moriyama et al[18] found a lower number of PCAs and a displacement of the entry site in highly myopic eyes compared with controls.

Apart from structural changes, the distribution of PSVs may represent a determining factor in the formation of choroidal watershed zones,[9] and the number of vessels per surface area might influence perfusion of the foveal outer retina.

Our results show a mean number of 0.33 submacular PSVs per mm^2. This quantification is possibly an important vascular characteristic of the human eye with relevance in health and disease. With the considerable variation in the eyes examined in this study, there is a need for validation of this finding in further investigations.

To our best knowledge, a quantification of PSVs in the submacular area has not been described before. The total number of SPCA branches piercing the sclera is reported with 5 to 20 in the literature.[19,20] However, this number comprises the paraoptic portion of vessels as well as the group of vessels distal to the optic nerve on the nasal and temporal side. Our submacular scan region would relate to the temporal distal portion of SPCAs only, which has not been separately reported.

Overall, there are only few reports published assessing PSVs, which would allow to put our data into perspective. Motaghiannezam et al[2] reported on choroidal vascular pattern by en face imaging using an swept-source OCT device in three subjects. Albeit not systematically assessing PSVs about the fovea, they depict the number of SPCAs in a 4- by 4-mm scan area in their work. By our calculation, this equals a mean number of 0.19 ± 0.06 PSVs per mm^2 in a comparable scan area, which is in the range of our finding.

In comparing the opposite subfields of the nasal, temporal, inferior, and superior quadrants, no pattern in distribution was found about the fovea. This would indicate an even arrangement of these vessels in the submacular area. In our emmetropic subjects, we found no dependency of vessel number on axial length in contrast to reported findings in myopic eyes.[18] Furthermore, fellow eyes included in this study showed no correlation in absolute vessel numbers in this small data set. This indicates a very low probability of vessel distribution to follow a symmetric pattern in fellow eyes.

We acknowledge several limitations of this study: There may be limited generalizability of our data set to, for example, older subjects, male subjects, or patient populations with disorders of the retina, choroid, or sclera. However, our study population is rather representative for young healthy women. Further studies should also include male volunteers, a wider range of age, and investigate a larger number of subjects.

The possibility of vessel-like artifacts imitating PSVs could lead to overestimation of their number. Linear hyporeflectivities at the level of the sclera can be caused by projection artifacts or possibly in combination with low signal-to-noise ratio. However, the three-dimensional approach described in this study, allowed for visualizing and tracking of PSVs from the sclera to the choroid. In many instances, the appearance of characteristic features such as branching, tortuosity, and continuity of an oblique scleral passage into the choroid is visible and makes the structures readily recognizable as vessels as shown in Figure 2. This can be used in the process of grading for differentiation from projection artifacts. In the assessment of healthy eyes, we do not expect other confounding structures or artifacts of relevance.

An underestimation of vessel number could be caused by the low signal-to-noise ratio at the deep level of the choroid and sclera. Averaging of more than 20 images per B-scan could help to further enhance the image quality. But this also significantly increases the total acquisition time per eye and is then limited by the patient's cooperation. In 2 of 22 eyes, no PSVs at all were visualized. This might be due to a true lack of vessels in the scanned area or an insufficient detection of deep vessel structures. However, the 12 μm slice spacing used seems sufficient for detection of vessels in the reported size of 50 μm to 200 μm.[2] Based on the three-dimensional visualization, future studies should also include quantitative assessment of the caliber and angle of insertion of PSVs.

In conclusion, EDI-SDOCT, in combination with the described postprocessing methods, pushes the boundaries of OCT imaging to a deeper, more posterior region of the eye. This allows for visualization and quantification of vessel structures crucial for outer retinal perfusion in the macula. This imaging modality is widely available, and relevant findings would be more readily transferable into studies and clinical practice. The application of next generation technologies can be expected to yield better imaging quality allowing to study the PSVs in more detail in health and disease and to follow changes over time.

Key words: enhanced depth imaging, EDI, OCT, perforating scleral vessels, posterior ciliary artery, choroid, sclera, imaging, speckle noise, choroidal perfusion.

References

1. Mrejen S, Spaide RF. Optical coherence tomography: imaging of the choroid and beyond. Surv Ophthalmol 2013;58:387–429.
2. Motaghiannezam R, Schwartz DM, Fraser SE. In vivo human choroidal vascular pattern visualization using high-speed swept-source optical coherence tomography at 1060 nm. Invest Ophthalmol Vis Sci 2012;53:2337–2348.
3. Spaide RF, Koizumi H, Pozzoni MC, Pozonni MC. Enhanced depth imaging spectral-domain optical coherence tomography. Am J Ophthalmol 2008;146:496–500.

4. Invernizzi A, Giani A, Cigada M, Staurenghi G. Retrobulbar structure visualization with enhanced depth imaging optical coherence tomography. Invest Ophthalmol Vis Sci 2013;54: 2678–2684.
5. Alm A, Bill A. Ocular and optic nerve blood flow at normal and increased intraocular pressures in monkeys (Macaca irus): a study with radioactively labelled microspheres including flow determinations in brain and some other tissues. Exp Eye Res 1973;15:15–29.
6. Parver LM, Auker C, Carpenter DO. Choroidal blood flow as a heat dissipating mechanism in the macula. Am J Ophthalmol 1980;89:641–646.
7. Gupta P, Saw SM, Cheung CY, et al. Choroidal thickness and high myopia: a case–control study of young Chinese men in Singapore. Acta Ophthalmol 2015;93:e585–e592.
8. Schmetterer L, Kiel J, eds. Ocular Blood Flow. Berlin, Heidelberg, Germany: Springer-Verlag, Berlin Heidelberg; 2012:3–21.
9. Hayreh SS. Posterior ciliary artery circulation in health and disease: the Weisenfeld lecture. Invest Ophthalmol Vis Sci 2004;45:749–757. 748.
10. Pedinielli A, Souied EH, Perrenoud F, et al. In vivo visualization of perforating vessels and focal scleral ectasia in pathological myopia. Invest Ophthalmol Vis Sci 2013;54:7637–7643.
11. Ohno-Matsui K, Akiba M, Ishibashi T, Moriyama M. Observations of vascular structures within and posterior to sclera in eyes with pathologic myopia by swept-source optical coherence tomography. Invest Ophthalmol Vis Sci 2012;53:7290–7298.
12. Querques G, Corvi F, Balaratnasingam C, et al. Lacquer cracks and perforating scleral vessels in pathologic myopia: a possible causal relationship. Am J Ophthalmol 2015;160:759–766.e2.
13. Maloca P, Gyger C, Schoetzau A, Hasler PW. Ultra-short-term reproducibility of speckle-noise freed fluid and tissue compartmentalization of the choroid analyzed by standard OCT. Transl Vis Sci Technol 2015;4:3.
14. Gyger C, Cattin R, Hasler PW, Maloca P. Three-dimensional speckle reduction in optical coherence tomography through structural guided filtering. Opt Eng 2014;53:073105.
15. Girard MJA, Strouthidis NG, Ethier CR, Mari JM. Shadow removal and contrast enhancement in optical coherence tomography images of the human optic nerve head. Invest Ophthalmol Vis Sci 2011;52:7738–7748.
16. Landis JR, Koch GG. An application of hierarchical kappa-type statistics in the assessment of majority agreement among multiple observers. Biometrics 1977;33:363.
17. Bates D, Mächler M, Bolker B, Walker S. Fitting linear mixed-effects models using lme4. 2014. arXiv preprint arXiv: 14065823.
18. Moriyama M, Ohno-Matsui K, Futagami S, et al. Morphology and long-term changes of choroidal vascular structure in highly myopic eyes with and without posterior staphyloma. Ophthalmology 2007;114:1755–1762.
19. Hayreh SS. The ophthalmic artery: III. Branches. Br J Ophthalmol 1962;46:212–247.
20. Susan S. Gray's Anatomy: The Anatomical Basis of Clinical Practice. Oxford, UK: Elsevier; 2015.